ORIGINAL ARTICLE

Homologous recombination deficiency is inversely correlated with microsatellite instability and identifies immunologically cold tumors in most cancer types

Jan Budczies[1,2,3,4*] (iD), Klaus Kluck[1], Susanne Beck[1], Iordanis Ourailidis[1], Michael Allgäuer[1], Michael Menzel[1], Daniel Kazdal[1,4] (iD), Lukas Perkhofer[3,5], Alexander Kleger[3,5], Peter Schirmacher[1,2,3], Thomas Seufferlein[3,5] and Albrecht Stenzinger[1,2,3,4*]

[1]Institute of Pathology, University Hospital Heidelberg, Heidelberg, Germany
[2]German Cancer Consortium (DKTK), Heidelberg, Germany
[3]Centers for Personalized Medicine (ZPM), Heidelberg and Ulm Partner Sites, Germany
[4]German Center for Lung Research (DZL), Heidelberg, Germany
[5]Department of Internal Medicine 1, University Hospital Ulm, Ulm, Germany

*Correspondence to: Jan Budczies, Institute of Pathology, University Hospital Heidelberg, Im Neuenheimer Feld 224, 69120 Heidelberg, Germany. E-mail: jan.budczies@med.uni-heidelberg.de and Albrecht Stenzinger, Institute of Pathology, University Hospital Heidelberg, Im Neuenheimer Feld 224, 69120 Heidelberg, Germany. E-mail: albrecht.stenzinger@med.uni-heidelberg.de

Abstract

Homologous recombination deficiency (HRD) leads to DNA double-strand breaks and can be exploited by the use of poly (ADP-ribose) polymerase (PARP) inhibitors to induce synthetic lethality. Extending the original therapeutic concept, the role of HRD is currently being investigated in clinical trials testing immune checkpoint blockers alone or in combination with PARP inhibitors, but the relationship between HRD and immune cell context in cancer is incompletely understood. We analyzed the association between immune cell composition, gene expression, and HRD in 9,041 tumors of 32 solid cancer types from The Cancer Genome Atlas (TCGA). The numbers of genomic scars were quantified by the HRD sum score (HRDsum) including loss of heterozygosity, large-scale state transitions, and telomeric allelic imbalance. The T-cell inflamed gene expression profile correlated weakly, but significantly positively, with HRDsum across cancer types ($\rho = 0.17$). Within individual cancer types, a significantly positive correlation was observed only in breast cancer, ovarian cancer, and four other cancer types, but not in the remaining 26 cancer types. HRDsum and tumor mutational burden (TMB) correlated significantly positively across cancer types ($\rho = 0.42$) and within 18 cancer types. HRDsum and a proliferation metagene correlated significantly positively across cancer types ($\rho = 0.52$) and within 20 cancer types. Mismatch repair deficiency and HRD as well as proof-reading deficiency showed a high level of exclusivity. High HRD scores were associated with an immunologically activated tumor microenvironment only in a minority of cancer types. Our data favor the combination of genetic markers, complex genomic markers (including HRDsum and TMB), and other molecular markers (including proliferation scores) for a precise and comprehensive read-out of the tumor biology and an individually tailored treatment.

Keywords: homologous recombination deficiency; HRD; microsatellite instability; MSI; PARP inhibitors; immune cell populations; T-cell inflamed gene expression profile; tumor mutational burden

Introduction

Defects in different components of the DNA repair machinery [1] are successfully exploited therapeutically in specific cancer types as well as across cancer types. Mismatch repair deficiency (MMRD) is typically detected by lack of immunohistochemical expression of MLH1, MSH2, MSH6, PMS2, or fragment length analysis indicating microsatellite instability (MSI). MMRD leads to accumulation of frameshift mutations connected with the expression of potent neoantigens. Deleterious mutations in *POLE* or *POLD1* lead to proofreading deficiency (PRD), accumulation of missense mutations, and ultra-high tumor mutational burden (TMB). Both MMRD and PRD represent promising biomarkers for responsiveness to immune checkpoint blockade (ICB) [2,3]. In 2017, the US Food and Drug Administration (FDA) approved pembrolizumab for the treatment of tumors with MMRD in an entity-agnostic manner. Additionally, in 2020, an entity-agnostic approval of TMB to detect patients who will likely benefit from ICB was granted [4,5].

Homologous repair deficiency (HRD), identified either by deleterious alterations of genes of the homologous recombination repair pathway or by the resulting signature of genomic scars, has been shown to identify patients who benefit from PARP inhibition [6–8].

More recent trials are investigating the role of HRD in the context of checkpoint blockade alone or in conjunction with PARP inhibition. The rationale behind this approach is the assumption that HRD, similar to MSI, may give rise to unstable genomes leading to neoantigens which elicit a strong immune response that could be unleashed by ICB. Combining ICB and PARP inhibitors may therefore result in additive or synergistic effects [9–14].

Over the last few years, many research efforts collectively led to an improved understanding of the immune cell context [15] in microsatellite unstable [16,17] and TMB-high [18] tumors, but studies comparing the immune cell composition in HRD-positive and -negative tumors are scarce. As a contribution to this research field, we comprehensively analyzed the association of HRD, MMRD/PRD, TMB, immune cell infiltration, and gene expression across 9,041 tumors of 32 solid cancer types. In this context, HRD was analyzed in two ways: (1) based on deleterious, biallelic mutations of *BRCA1/2* and *BRCA1* hypermethylation and (2) based on HRDsum, the summation score of loss of heterozygosity (LOH) [19], large-scale state transitions (LSTs) [20], and telomeric allelic imbalance (TAI) [21] recently used in clinical trials [8].

Materials and methods

The analysis was performed using data from The Cancer Genome Atlas (TCGA) and comprised 9,041 primary tumors of 32 solid cancer types. Leukemia cases were excluded. Only tumors with both mutational data (from whole-exome sequencing) and copy number data (from single-nucleotide polymorphism [SNP] arrays) were included. Gene expression data were available for 8,522 of these tumors.

Allele-specific copy numbers estimated from SNP array data using the ASCAT algorithm were obtained from the GDC Data Portal [22]. Starting from the copy number data, HRD scores, LOH, LST, TAI, and HRDsum ($=$ LOH + LST + TAI) were calculated using scarHRD [23].

Gene expression data and mutation calls were obtained from the pan-cancer web page of the GDC Data Portal (https://gdc.cancer.gov/about-data/publications/pancanatlas). Gene expression data were transformed to a logarithmic scale using the transformation x to $\log2(x + 1)$. The abundance of 14 specific immune cell populations in the tumor microenvironment (TME) was estimated using the method developed by Danaher et al. [24]. The level of the T-cell inflamed gene expression profile (GEP) was calculated as described in [25].

TMB was calculated by counting the missense mutations of each tumor. The cutoff points of 42 genomic scars and 199 missense mutations (corresponding to 10 mut/Mb) were used for stratification of HRDsum and TMB values, respectively [8,26,27]. Ultra-high TMB was defined by the cutoff point of 1,990 missense mutations (corresponding to 100 mut/Mb) [28].

Statistical analysis and generation of figures were performed using the statistical programming language R. Associations between continuous variables were assessed using Spearman correlations (ρ). Associations between continuous variables and binary variables were assessed using the two-sided Wilcoxon test. Association between dichotomized versions of the biomarkers (binary variables) was assessed using the two-sided Fisher's exact test. Multiple testing correction was carried out using the Benjamini–Hochberg method to control the false discovery rate (FDR) at 10%. In the context of heatmap display, multiple testing correction included both dimensions, the cancer types, and the immune biomarkers.

The association of HRDsum and gene expression of individual genes was assessed using Spearman correlations and corresponding P values. Separate gene lists of positively ($\rho > 0.3$) and of negatively ($\rho < -0.3$) correlating genes were generated. Only genes that

were significant after multiple testing correction (Benjamini–Hochberg method, FDR = 10%) were included in the gene lists. The gene lists were analyzed for enrichment with respect to the 50 hallmark gene sets from the Molecular Signatures Database (MSigDB v7.4) [29]. The significance of enrichments or depletions was assessed using the two-sided Fisher's exact test. The enrichment foldchange with respect to a hallmark gene set was calculated as quotient of the proportion of the genes in the gene list in the gene set divided by the proportion of the genes in the genome in the gene set. A proliferation metagene was defined as mean expression level (log2 scale data) of the 200 genes in the 'G2M-checkpoint' hallmark gene set.

Results

A total number of 9,041 primary tumors of 32 solid cancer types were included. A list of cancer type abbreviations used in the description and discussion of the data is provided in Table 1.

Association of immune cell infiltration with HRD
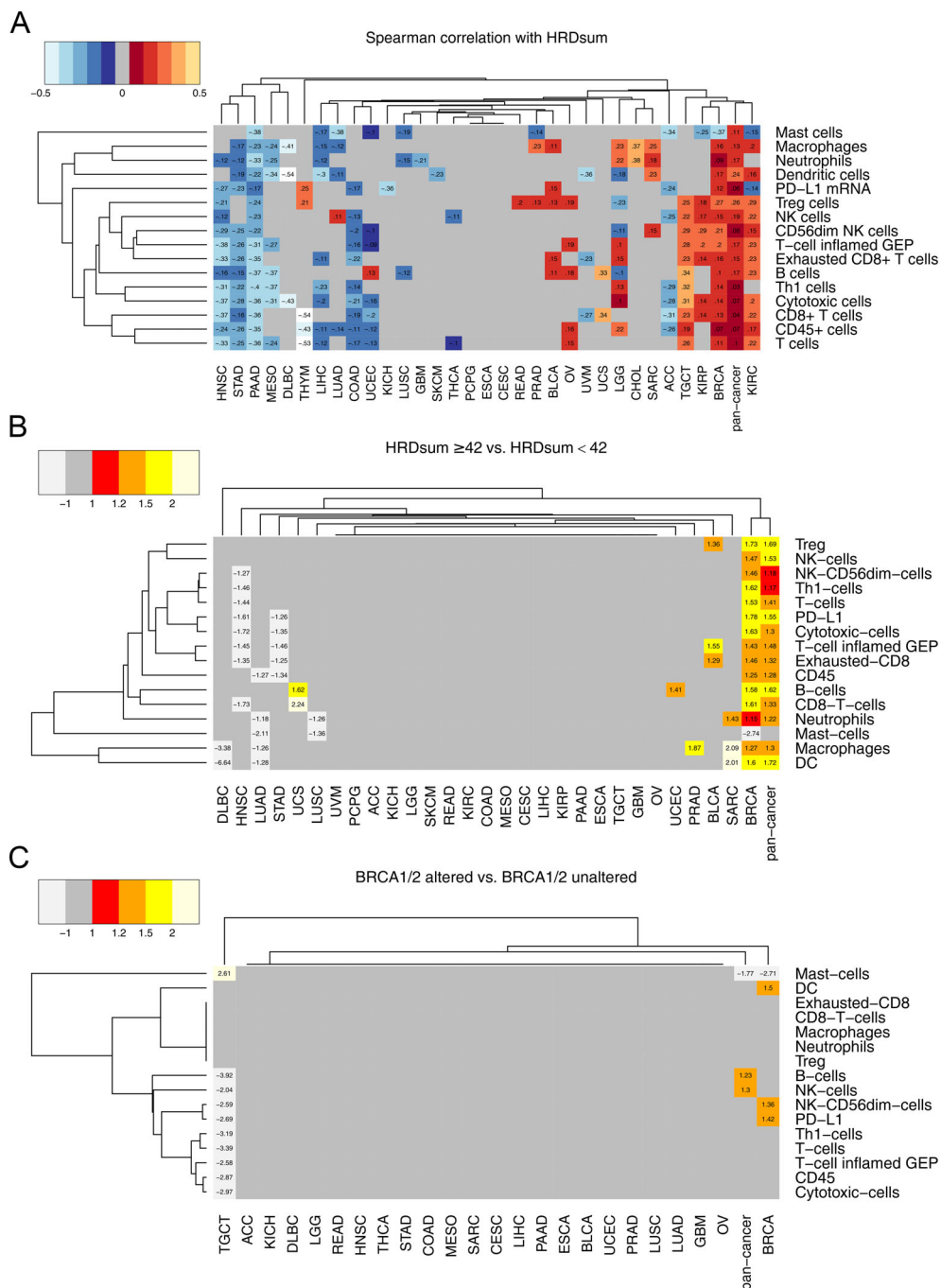
HRDsum as a continuous variable

We analyzed the association of 14 specific immune cell populations, PD-L1 expression, and the T-cell inflamed GEP with HRDsum (Figure 1). The T-cell inflamed GEP correlated weakly, but significantly positively, with HRDsum across cancer types ($\rho = 0.17$) as well as in the following cancer types: BRCA, KIRC, KIRP, LGG, OV, and TGCT ($\rho = 0.20, 0.23, 0.20, 0.10, 0.19,$ and 0.28). For the remaining cancer types, no significant positive correlation was observed. When analyzing the aggregated pan-cancer dataset, HRDsum also correlated positively with a core set of immune cell populations including CD8-positive T cells, regulatory T cells, and NK cells (Figure 1A). This was also observed in four of the mentioned cancer types (BRCA, KIRC, KIRP, and TGTC). In 11 other cancer types (BLCA, CHOL, OV, LGG, LUAD, PRAD, READ, THYM, SARC, UCEC, and UCS) positive correlations were detected only for a minority (1–7) of the immune markers. In the majority of cancer types (17 of 32), none of the immune cell populations correlated significantly positively with HRDsum.

Table 1. Cancer type abbreviations

ACC	Adrenocortical carcinoma
BLCA	Bladder urothelial carcinoma
BRCA	Breast invasive carcinoma
CESC	Cervical squamous cell carcinoma and endocervical adenocarcinoma
CHOL	Cholangiocarcinoma
COAD	Colon adenocarcinoma
DLBC	Diffuse large B-cell lymphoma
ESCA	Esophageal carcinoma
GBM	Glioblastoma multiforme
HNSC	Head and neck squamous cell carcinoma
KICH	Kidney chromophobe
KIRC	Kidney renal clear cell carcinoma
KIRP	Kidney renal papillary cell carcinoma
LGG	Brain lower grade glioma
LIHC	Liver hepatocellular carcinoma
LUAD	Lung adenocarcinoma
LUSC	Lung squamous cell carcinoma
MESO	Mesothelioma
OV	Ovarian serous cystadenocarcinoma
PAAD	Pancreatic adenocarcinoma
PCPG	Pheochromocytoma and paraganglioma
PRAD	Prostate adenocarcinoma
READ	Rectum adenocarcinoma
SARC	Sarcoma
SKCM	Skin cutaneous melanoma
STAD	Stomach adenocarcinoma
TGCT	Testicular germ cell tumors
THYM	Thymoma
THCA	Thyroid carcinoma
UCS	Uterine carcinosarcoma
UCEC	Uterine corpus endometrial carcinoma
UVM	Uveal melanoma

HRDsum as a dichotomized variable

Comparing HRD-positive and HRD-negative tumors (cutoff point: 42 genomic scars), a significantly higher T-cell inflamed GEP was detected in the aggregated pan-cancer dataset (fold change = 1.48). In the analysis of the 32 individual cancer types, a higher T-cell inflamed GEP was detected only in bladder cancer (BLCA, fold change = 1.55) and in breast cancer (BRCA, fold change = 1.43), but in none of the other cancer types. In the pan-cancer dataset and in BRCA, all investigated immune cell populations with the exception of mast cells were up-regulated simultaneously with the GEP. In BLCA, PRAD, SARC, UCEC, and UCS, we detected up-regulation of a few immune cell populations in HRD-positive tumors, while none of the 14 immune cell populations were up-regulated in the remaining 26 cancer types (Figure 1B). In SARC, we observed a strong up-regulation of macrophages and of dendritic cells (both fold changes > 2). Up-regulation of cytotoxic cells and of PD-L1 was detected only pan-cancer (fold changes = 1.3 and 1.55) and in BRCA (fold changes = 1.63 and 1.78), but in none of the 31 other cancer types.

Figure 1. Association of the levels of specific immune cell populations, PD-L1 expression, and the T-cell inflamed GEP with the HRDsum score across cancer types (pan-cancer) and in each of 32 cancer types. (A) Heatmap of Spearman correlations between HRDsum and the gene expression-based biomarkers. (B) Heatmap of fold changes between HRD-positive (HRDsum ≥ 42) and HRD-negative (HRDsum < 42) tumors. (C) Heatmap of fold changes between *BRCA1/2*-altered tumors and the remaining tumors. Alterations included comprised deleterious biallelic mutations in *BRCA1* or *BRCA2* and *BRCA1* hypermethylation. Colored boxes mark results that were significant after multiple testing correction for both the investigated cancer types and the investigated biomarkers (33 × 16 hypotheses, FDR = 10%). Dark grey boxes mark not significant results.

HRD interrogated by the mutational status of *BRCA1/2*

Comparing tumors with deleterious alterations in *BRCA1/2* and unaltered tumors, immune up-regulation was only observed in breast cancer, in testicular germ cell cancer, and in the pan-cancer analysis and restricted to very few biomarkers (Figure 1C).

Analysis of HRDsum in the subtypes of breast cancer and ovarian cancer

The highest levels of HRDsum were detected in triple-negative breast cancer (TNBC), high-grade serous ovarian carcinoma, and low-grade serous ovarian carcinoma (supplementary material, Figure S1A). The levels of HRDsum were lower in HER2+ breast cancer and even lower in hormone receptor positive (HR+) HER2− breast cancer. Positive correlations of the T-cell inflamed GEP and a few immune cell populations were detected in HR+/HER2− breast cancer, but not in the other subtypes of breast cancer and not in the subtypes of ovarian cancer (supplementary material, Figure S1B). Up-regulation of almost all immune markers (except B cells and mast cells) was detected in the HRD-positive tumors of HR+/HER2− breast cancer (supplementary material, Figure S1C). Only two immune cell populations were up-regulated in the HRD-positive tumors of HER2+ breast cancer, while none of the immune markers were up-regulated in the HRD-positive tumors of TNBC and of the subtypes of ovarian cancer.

Functional genomics analysis of HRD scores

We carried out a genome-wide correlation analysis of gene expression and HRDsum followed by a gene set enrichment analysis. Correlating genes were investigated across cancer types and separately for each of the cancer types. Gene lists of significantly correlating genes were generated separately for positive and for negative correlations and only genes with correlations above the threshold $|\rho| > 0.3$ were include in the lists. Significant correlations between GEPs and HRDsum were detected across cancer types and in 29 of 32 cancer types (Figure 2A). Across cancer types, there were 1,072 genes (5.2% of all genes) in the list of positively correlating genes and 511 genes (2.5% of all genes) in the list of negatively correlating genes.

The gene lists were analyzed for enrichment with respect to the 50 hallmark gene sets from the Molecular Signatures Database [29]. We detected 112 (6.8%) enriched categories and 103 (6.2%) depleted categories for the positively correlating

genes in a total of $33 \times 50 = 1,650$ analyses (Figure 2B). For the negatively correlating genes, we detected 54 (3.3%) enriched categories and 25 (1.5%) depleted categories. Enrichment of the category 'G2M_CHECKPOINT' for the positively correlating genes was detected across cancer types and for 16 cancer types (ACC, BLCA, BRCA, KIRC, KIRP, LGG, LIHC, LUAD, LUSC, MESO, PAAD, PCPG, PRAD, SKCM, SARC, and UCEC). In 14 of these cancer types, we additionally observed enrichment of the category 'E2F_TARGETS' and in 12 of these cancer types of the category 'MITOTIC_SPINDLE'. Thus, cell cycle related genes were over-represented among the positive correlators of HRDsum in half of the cancer types under investigation.

The correlation of HRDsum with the 200 genes in the category 'G2M_checkpoint' in each of the cancer types was visualized as a heatmap (Figure 3). Clustering revealed a cluster of 14 cancer types and a corresponding cluster of 110 genes showing consistently positive correlations between HRDsum and gene expression.

Correlation of HRDsum scores with TMB and with proliferation rates

Correlation of HRDsum with TMB and with proliferation was analyzed pan-cancer and within each of the cancer types. Pan-cancer, a positive correlation was detected between HRDsum and TMB ($\rho = 0.42$, $p < 2.2\text{E-}16$, Figure 4A). Within specific cancer types, HRDsum and TMB correlated significantly positively in 18 cancer types (Figure 4C), with the strongest correlations ($\rho \geq 0.35$) detected in the 10 cancer types ACC, BLCA, BRCA, LGG, LUAD, OV, PAAD, PRAD, SARC, and THYM. Significantly negative correlations were detected in COAD and UCEC ($\rho = -0.33$ and $\rho = -0.37$) connected with a considerable prevalence of tumors with MMRD and PRD in these entities (COAD: 6% and 17%, UCEC: 31% and 14%). Excluding tumors with MMRD or PRD, correlations between HRDsum and TMB were not significant in COAD and significantly positive in UCEC ($\rho = 0.23$).

Proliferation was quantified by a metagene defined as the mean expression level of the 200 genes in the 'G2M-checkpoint' hallmark gene set. Across cancer types, a positive correlation was detected between HRDsum and the proliferation metagene ($\rho = 0.52$, $p < 2.2\text{E-}16$, Figure 4B). HRDsum and proliferation correlated significantly positively in 21 cancer types (Figure 4C), with the strongest correlations ($\rho \geq 0.35$)

A

B   C
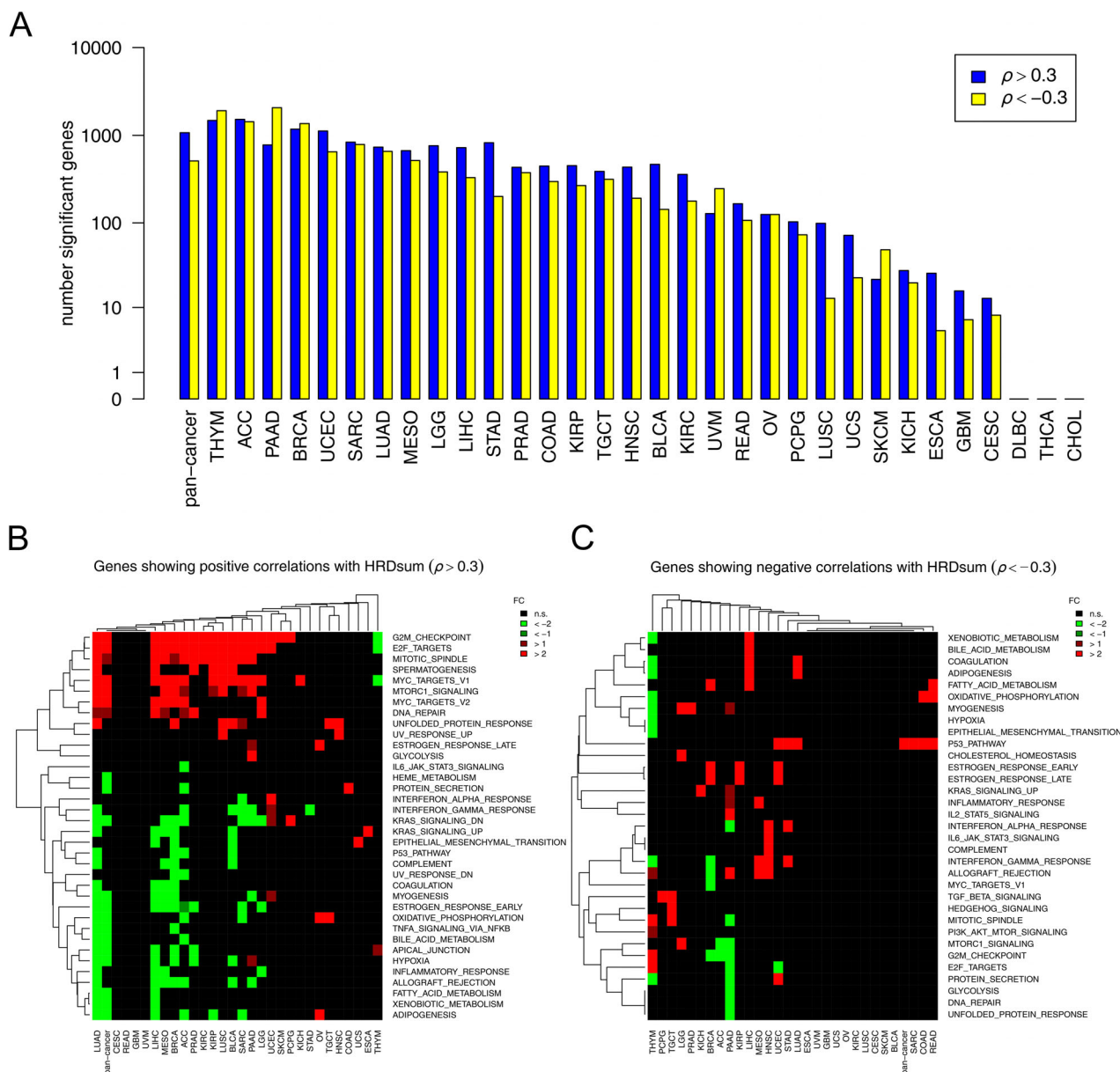
Figure 2. Correlation analysis of the genome-wide expression pattern with HRDsum. For each cancer type, lists of significantly (FDR = 10%) positively and negatively correlated genes were generated and functionally analyzed. Only genes with a correlation $|\rho| > 0.3$ were included in the lists. (A) Numbers of genes in the lists of positively and negatively correlated genes. (B) Enrichment analysis of the list of positively correlated genes with respect to the categories in the hallmarks gene sets of MSigDB. (C) Same as in (B), but for the negatively correlated genes. Colored (green = enrichment, red = depletion) boxes mark results that were significant after correction for both the investigated 33 cancer types and the 50 investigated hallmarks (33 × 50 hypotheses, FDR = 10%). The enrichment fold changes (FC) displayed in the heatmap are defined as quotient of the proportion of the genes in the gene list annotated for the functional category under consideration divided by the proportion of the genes in the genome annotated for the functional category.

detected in the 10 cancer types ACC, BLCA, BRCA, KIRP, LIHC, LUAD, MESO, PAAD, PRAD, and SARC. A significantly negative correlation between HRDsum and proliferation was detected in THYM ($\rho = -0.37$).

We calculated the partial correlation between HRDsum and TMB controlling for the level of the proliferation metagene. Pan-cancer, the correlation dropped from $\rho = 0.52$ to a lower, but still highly significant value of $\rho = 0.24$ ($p = 4.5E\text{-}111$) after the
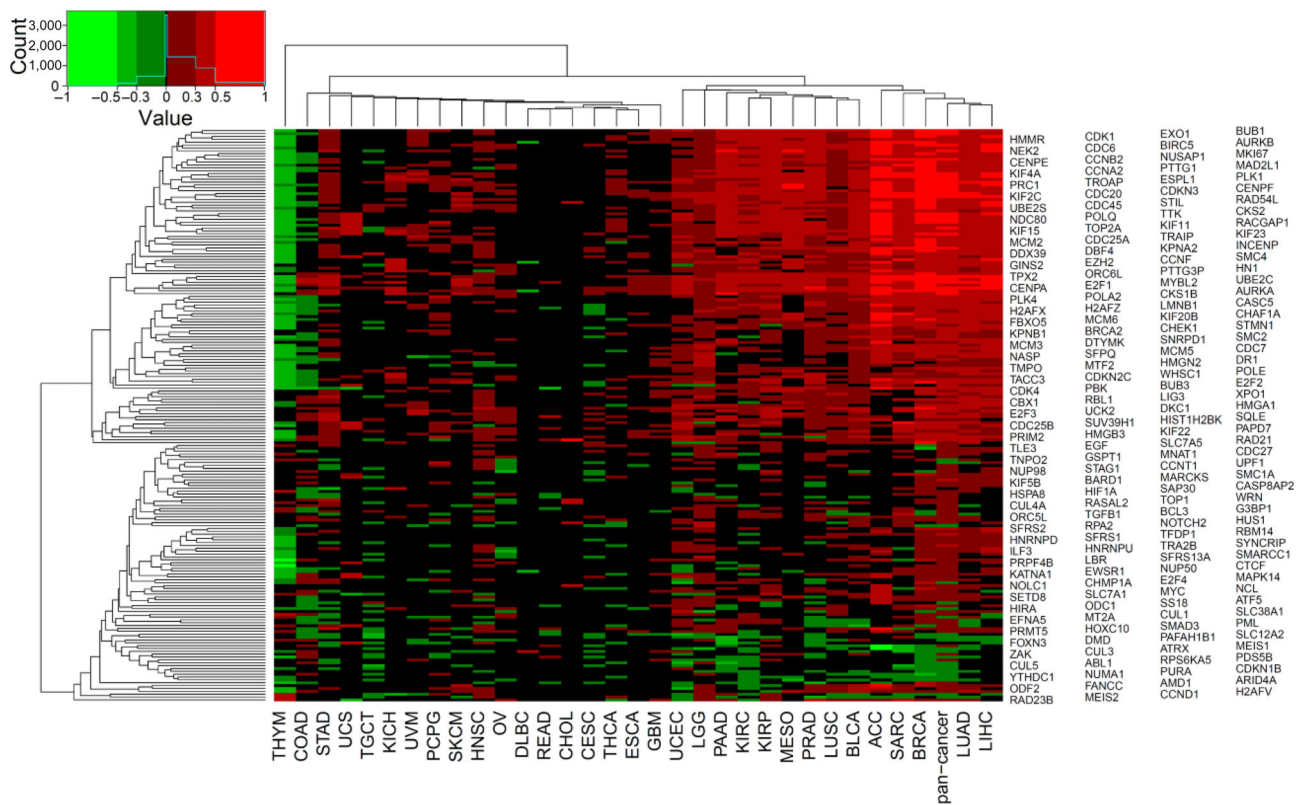
Figure 3. Correlation analysis of HRDsum and the mRNA expression of 200 genes involved in the regulation of the G2/M checkpoint of the cell cycle (hallmark gene set G2M_CHECKPOINT). The heatmap shows the levels of Spearman correlations across cancer types and in each of 32 specific cancer types. The genes in the top cluster (110 genes) show significantly positive correlation with HRDsum across cancer types and in each of the 14 cancer types in the right cluster: in ACC, BLCA, BRCA, KIRC, KIRP, LGG, LIHC, LUAD, LUSC, MESO, PAAD, PRAD, SARC, and UCEC. Colored boxes mark significant correlations (red = positive correlations, green = negative correlations). Black boxes mark not significant correlations.

control for proliferation. For 17 of the 21 cancer types with a significantly positive correlation between HRDsum and TMB, we detected a numerically lower correlation after controlling for proliferation (Figure 4C). These observations are in line with the hypothesis that high proliferation gives rise to a high number of mutations and contributes to both high HRDsum scores and high TMB.

Tumor classification by HRDsum and TMB

HRDsum with a cutoff point of 42 is an FDA- and European Medicines Agency (EMA)-approved biomarker to select ovarian cancer patients for PARP inhibition [8]. TMB with a cutoff point of 10 mut/Mb is an FDA-approved entity-overarching biomarker to select patients for pembrolizumab monotherapy [30]. To estimate the number of patients that these biomarkers would select for the respective therapies, we calculated the numbers of HRD-positive, TMB-positive, and double-positive patients

for each of the cancer types (Figure 5). Additionally, we stratified the tumors with respect to the level of tumor cell proliferation. The quantification of proliferation was based on the expression of a metagene including the 200 genes in the hallmark gene set G2M_CHECKPOINT.

Across cancer types, 1,695 (18.7%) tumors were classified as HRD-positive, while 1,291 (14.3%) tumors were classified as TMB-high. The highest proportions of HRD-positive tumors were detected in OV (70%), LUSC (52%), ESCA (44%), UCS (41%), SARC (39%), and LUAD (35%). The highest percentages of TMB-high tumors were detected in SKCM (60%), LUSC (50%), LUAD (45%), UCEC (37%), and BLCA (36%). The percentage of tumors that were neither HRD- nor TMB-positive varied strongly across cancer types: While less than 50% of the tumors were double-negative in BLCA, LUAD, LUSC, SKCM, STAD, OV, and UCEC, more than 95% of tumors were double-negative in CHOL, GBM, KIRC, KIRP,
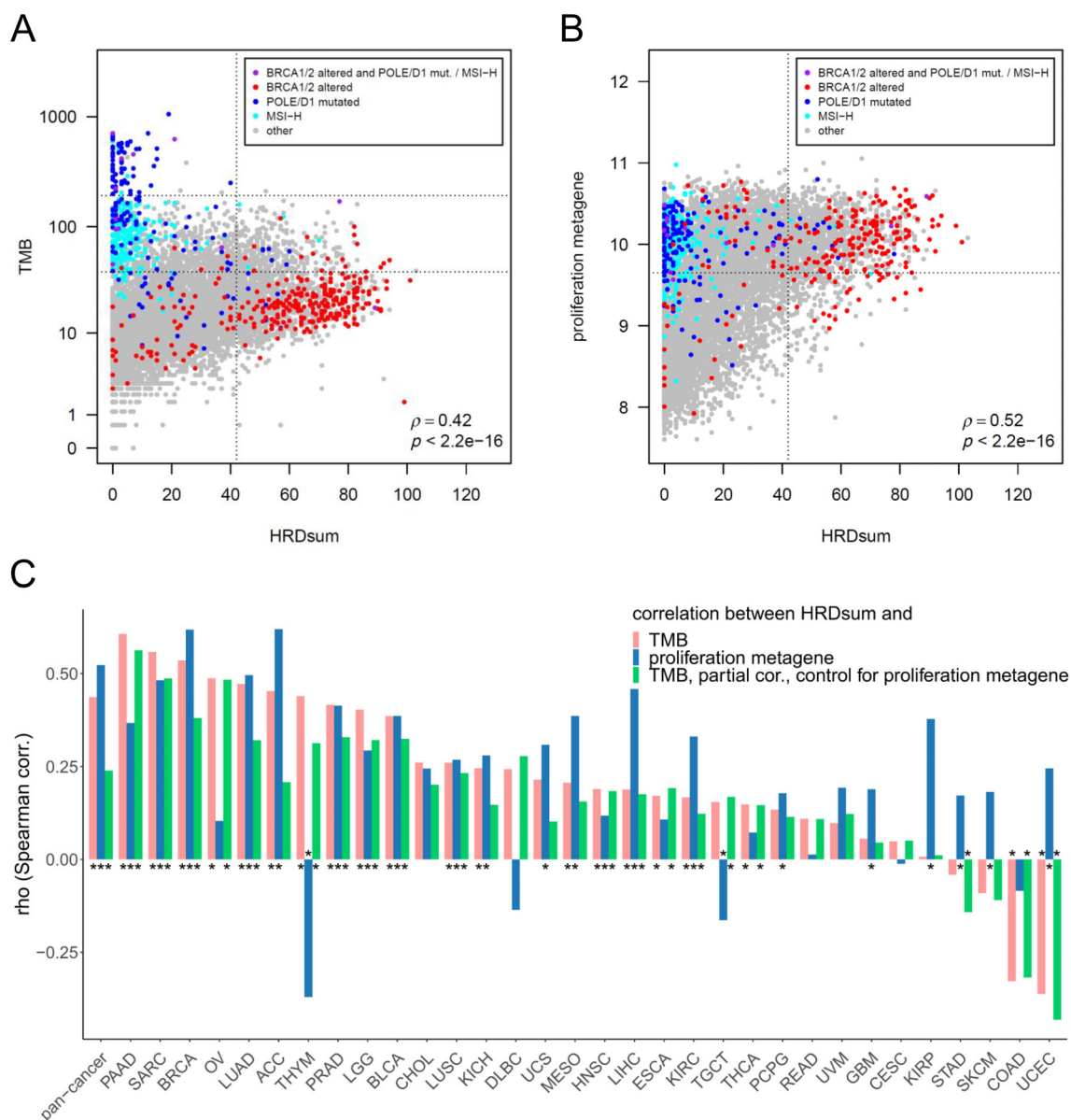
Figure 4. Analysis of the correlations of HRDsum with TMB and with the proliferation level in 9,041 tumors of 32 cancer types. (A) Association of the levels of HRDsum and TMB with *BRCA1/2*, MSI, and *POLE/D1* status in the pan-cancer dataset. (B) Same as in (A), but for the levels of HRDsum and proliferation. Proliferation was quantified by the mean expression level of 200 genes annotated to the G2M checkpoint. (C) Correlation analysis of (1) HRDsum and TMB, (2) HRDsum and proliferation, and (3) HRDsum and TMB controlled for the level of proliferation (partial correlation) across cancer types and in each of the 32 cancer types. Significant correlations after multiple testing correction for the investigated cancer types and the three different analyses (33×3 hypotheses, FDR = 10%) are marked by stars.

KICH, LGG, PCPG, PRAD, TGCT, THCA, THYM, and UVM. In 9 of these 12 cancer types (in all apart from GMB, TGCT, and THYM) with a very high percentage of double-negative tumors, low-proliferating tumors were abundant with 85% or more.

Across cancer types, simultaneous high TMB and high HRDsum were detected in 4.3% of the tumors, which is significantly higher than the expected overlap of 2.7% for independent variables ($p = 6.4E-16$). The highest prevalences of tumors with high levels of both genomic markers were detected in LUSC (30%),
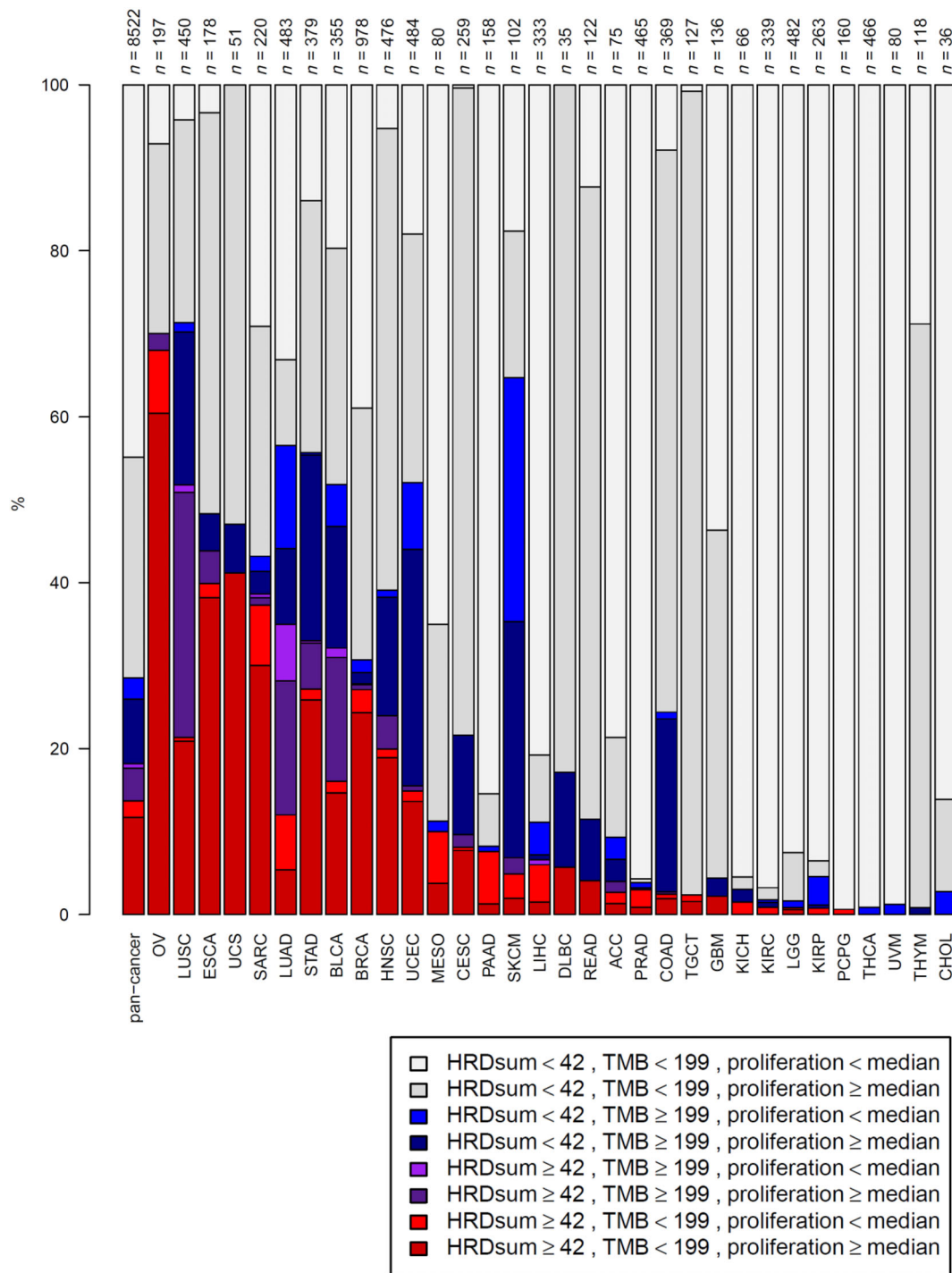
Figure 5. Tumor classification by HRDsum, TMB, and proliferation level. Proportions of HRD-positive (HRDsum ≥ 42) tumors, hypermutated (TMB ≥ 10 mut/Mb) tumors, and strongly proliferating (proliferation metagene ≥ median) tumors across cancer types and for each of the 32 cancer types. Brighter colors denote strongly proliferating tumors, while darker colors denote weakly proliferating tumors.

LUAD (23%), BLCA (16%), STAD (5.8%), and HNSC (4.0%). In none of these cancer types did we detect a significantly higher level of any of the immune markers in the tumors with high TMB and

HRDsum compared to the tumors with high TMB and low HRDsum (data not shown). Thus, using HRDsum additionally to TMB did not improve the identification of highly immune-infiltrated tumors.

HRD is inversely correlated with MSI

Ultra-hypermutation as commonly defined by a TMB above 100 mut/Mb [28] was detected in 81 (0.9%) tumors of the study cohort. Out of these, only a single tumor had HRDsum ≥ 42, reflecting a high level of exclusivity of ultra-hypermutation and HRD (p = 2.6E-06). We also analyzed the association of HRD with MMRD and PRD using the MSI status determined by the Bethesda assay (available for COAD, READ, STAD, and UCEC) as marker for MMRD and using mutations in the exonuclease domain of *POLE* or *POLD1* as markers for PRD. Using these markers, 297 (3.3%) tumors of the study cohort were classified as MMR-deficient, while 172 (1.9%) tumors were classified as proofreading-deficient. We detected a high level of exclusivity of HRD and MMRD as well as HRD and PRD, as only 4 (0.05%, p < 2.2E-16) and 15 tumors (0.18%, p = 0.00064) tumors were deficient for both DNA repair systems. These results are in line with a high level of exclusivity of deficiency in different DNA repair systems in cancer cells.

Discussion

Following preclinical work, a number of clinical trials are currently investigating the combined use of PARP inhibition and checkpoint blockade across solid cancer types as well as in specific cancers, such as ovarian cancer, breast cancer, prostate cancer, and cholangiocarcinoma [9]. The conceptual approach is based on several major observations: (1) Tumors with high mutational load, which is associated with a higher likelihood of neoantigens [4], tend to harbor functionally abrogative mutations in genes implicated in DNA repair mechanisms including homologous recombination repair [13,31,32]; (2) Preclinical evidence that tumor cells with genomic instability may accumulate tumor-derived double-stranded DNA in the cytoplasm, which can lead to activation of the cGAS-STING pathway leading to a type I interferon-mediated anti-tumor immune response [33–39]; (3) Data suggesting that defects in *BRCA1/2* as well as PARP inhibition itself can be associated with higher PD-L1 levels [40,41]; and (4) PARP inhibition may shape the TME from a passively inflamed state, influenced by suppressive immune cells, toward a proactive tumor immune response [41,42].

But, clinical data on combination therapy approaches are still limited and the associations between tumors exhibiting HRD and the immune microenvironment and other genetic aberrations are still poorly understood. Importantly, while a given set of cancer types might display some level of genomic instability, the underlying mechanisms may differ and play a crucial role as these lead to different genetic aberrations in the tumor genome, which in turn influences the immune contexture. Utilizing the TCGA dataset comprising 9,041 cases, this study analyzed the association of HRD with TMB, with immune cell populations, with T-cell inflamed GEP as well as with genome-wide GEPs.

Notably, positive associations between the T-cell inflamed GEP and HRDsum were detected only in the following six cancer types: BRCA, OV, LGG, TGCT, KIRC, and KIRP. Only four of them (BRCA, TGCT, KIRC, and KIRP) also demonstrated positive correlations with a core set of immune cells implicated in anti-tumor response. The analysis of the aggregated pan-cancer dataset showed only a weak correlation that is driven by the aforementioned cancer types as well as individual cases form other entities. Higher expression of *PD-L1* in HRD-positive tumors was observed only pan-cancer and in breast cancer. When stratifying tumors based on deleterious *BRCA1/2* alterations instead of HRDsum, the absence of an association with an immunological active TME was even more pronounced; significant associations were detected only for breast cancer and testicular germ cell tumors, but not for the remaining 30 cancer types. Taken together, with the exception of breast and bladder cancer, for which tumors with HRDsum ≥ 42 showed an increased T-cell inflamed GEP and upregulated immune cell populations, the majority of cancer types displaying HRD appear to be immunologically cold and require therapeutic modulation toward an activated TME. As the association of immune cell markers with HRD is differently pronounced in different cancer types, a tumor type-specific rather than an entity-agnostic approach might be appropriate for establishing HRDsum as a marker for immune therapy guidance.

In the study cohort, only 4.3% of the tumors were characterized by simultaneous HRD-positivity and a TMB-high status, both of which were defined according to approved biomarkers derived from prospective clinical trials with a cutoff point of 42 for the HRDsum score [8] and a cutoff point of 10 mut/Mb for TMB [27]. At the same time, a total of 14.3% of the tumors had high TMB. Consistent with biological considerations, these results suggest that HRD is not a major driver of TMB. In this context, it is also important to note that MMRD and defective *POLE/POLD1*, which both give rise to ultra-high TMB counts, potent neoantigens [3,43,44], and indicate responsiveness to pembrolizumab, are mutually exclusive with HRD.

Gene expression analysis revealed a positive correlation of genes implicated in cell cycle regulation and proliferation with HRDsum in 21 cancer types. The

association between HRD and high proliferation rates [45] is likely explainable by the accumulation of genomic scars over a high number of cell divisions and a high likelihood of DNA double-strand breaks and imperfect DNA repair during mitosis. Stochastically, highly proliferating tumors might also impair immune response through (1) replication exceeding immune-mediated detection and subsequent killing of tumor cells and (2) molecular evolution leading to immune evasion. The retinoblastoma (RB) pathway appears to play a role in this context [46]. As the RB pathway supports the repair of DNA double-strand breaks by non-homologous end-joining [47,48], there might be a rationale in exploring the effect of PARP inhibition and modulation of the RB pathway in preclinical models. Interestingly, a recent study observed that the loss of RB in the HRD-high subgroup of high-grade serous ovarian cancers was associated with prolonged survival, increased CD8+ T cells, and higher proliferation [49].

Limitations of our study are the fact that our analysis is primarily based on resected tumor specimens with molecular data, which are not spatially resolved, and the absence of a validation cohort. Furthermore, the investigated tissue samples represent a balance between immune response, immune-editing of the tumor, and immune evasion in the absence of treatment. Thus, the study cannot identify the effect of PARP inhibition or combined PARPi and ICB on the immune cell context nor directly assess the role of biomarkers in this context.

In conclusion, our study provides a comprehensive overview of the associations between HRD, MMRD, PRD, and TMB as well as the immune cell context and GEPs in ICB/PARPi-naïve tumors, which invites consideration of these findings in the design of clinical trials as well as preclinical disease models.

Acknowledgements

Author contributions statement

JB was involved in conceptualization, methodology, software, formal analysis, visualization, writing – original draft, writing – review and editing, supervision, project administration and funding acquisition. KK, SB and IO made substantial contributions to software, data curation, formal analysis, visualization and writing – review and editing. MA was responsible for writing – original draft and writing – review and editing. MM, DK, LP, AK and PS were involved in writing – review and editing. TS was responsible for conceptualization and writing – review and editing. AS made substantial contributions to conceptualization, writing – original draft, writing – review and editing, supervision, project administration and funding acquisition.

References

1. Hanahan D, Weinberg RA. Hallmarks of cancer: the next generation. *Cell* 2011; **144**: 646–674.

2. Le DT, Durham JN, Smith KN, *et al*. Mismatch repair deficiency predicts response of solid tumors to PD-1 blockade. *Science* 2017; **357**: 409–413.

3. André T, Shiu KK, Kim TW, *et al*. Pembrolizumab in microsatellite-instability-high advanced colorectal cancer. *N Engl J Med* 2020; **383**: 2207–2218.

4. Sha D, Jin Z, Budczies J, *et al*. Tumor mutational burden as a predictive biomarker in solid tumors. *Cancer Discov* 2020; **10**: 1808–1825.

5. Marabelle A, Fakih M, Lopez J, *et al*. Association of tumour mutational burden with outcomes in patients with advanced solid tumours treated with pembrolizumab: prospective biomarker analysis of the multicohort, open-label, phase 2 KEYNOTE-158 study. *Lancet Oncol* 2020; **21**: 1353–1365.

6. Miller RE, Leary A, Scott CL, *et al*. ESMO recommendations on predictive biomarker testing for homologous recombination deficiency and PARP inhibitor benefit in ovarian cancer. *Ann Oncol* 2020; **31**: 1606–1622.

7. Lord CJ, Ashworth A. PARP inhibitors: synthetic lethality in the clinic. *Science* 2017; **355**: 1152–1158.

8. Ray-Coquard I, Pautier P, Pignata S, *et al*. Olaparib plus bevacizumab as first-line maintenance in ovarian cancer. *N Engl J Med* 2019; **381**: 2416–2428.

9. Peyraud F, Italiano A. Combined PARP inhibition and immune checkpoint therapy in solid tumors. *Cancers (Basel)* 2020; **12**: 1502.

10. van Wilpe S, Tolmeijer SH, Koornstra RHT, *et al*. Homologous recombination repair deficiency and implications for tumor immunogenicity. *Cancers (Basel)* 2021; **13**: 2249.

11. Hsiehchen D, Hsieh A, Samstein RM, *et al*. DNA repair gene mutations as predictors of immune checkpoint inhibitor response beyond tumor mutation burden. *Cell Rep Med* 2020; **1**: 100034.

12. Färkkilä A, Gulhan DC, Casado J, *et al*. Immunogenomic profiling determines responses to combined PARP and PD-1 inhibition in ovarian cancer. *Nat Commun* 2020; **11**: 1459.

13. Brown JS, Sundar R, Lopez J. Combining DNA damaging therapeutics with immunotherapy: more haste, less speed. *Br J Cancer* 2018; **118**: 312–324.

14. Pilié PG, Gay CM, Byers LA, *et al*. PARP inhibitors: extending benefit beyond BRCA-mutant cancers. *Clin Cancer Res* 2019; **25**: 3759–3771.

15. Giraldo NA, Sanchez-Salas R, Peske JD, *et al*. The clinical role of the TME in solid cancer. *Br J Cancer* 2019; **120**: 45–53.

16. Maby P, Bindea G, Mlecnik B, *et al*. License to kill: microsatellite instability and immune contexture. *Oncoimmunology* 2021; **10**: 1905935.

17. Shin SJ, Kim SY, Choi YY, *et al*. Mismatch repair status of gastric cancer and its association with the local and systemic immune response. *Oncologist* 2019; **24**: e835–e844.

18. Budczies J, Seidel A, Christopoulos P, *et al*. Integrated analysis of the immunological and genetic status in and across cancer types: impact of mutational signatures beyond tumor mutational burden. *Oncoimmunology* 2018; **7**: e1526613.

19. Abkevich V, Timms KM, Hennessy BT, *et al*. Patterns of genomic loss of heterozygosity predict homologous recombination repair defects in epithelial ovarian cancer. *Br J Cancer* 2012; **107**: 1776–1782.

20. Popova T, Manié E, Rieunier G, *et al*. Ploidy and large-scale genomic instability consistently identify basal-like breast carcinomas with BRCA1/2 inactivation. *Cancer Res* 2012; **72**: 5454–5462.

21. Birkbak NJ, Wang ZC, Kim JY, *et al*. Telomeric allelic imbalance indicates defective DNA repair and sensitivity to DNA-damaging agents. *Cancer Discov* 2012; **2**: 366–375.

22. Grossman RL, Heath AP, Ferretti V, *et al*. Toward a shared vision for cancer genomic data. *N Engl J Med* 2016; **375**: 1109–1112.

23. Sztupinszki Z, Diossy M, Krzystanek M, *et al*. Migrating the SNP array-based homologous recombination deficiency measures to next generation sequencing data of breast cancer. *NPJ Breast Cancer* 2018; **4**: 16.

24. Danaher P, Warren S, Dennis L, *et al*. Gene expression markers of Tumor Infiltrating Leukocytes. *J Immunother Cancer* 2017; **5**: 18.

25. Ayers M, Lunceford J, Nebozhyn M, *et al*. IFN-γ-related mRNA profile predicts clinical response to PD-1 blockade. *J Clin Invest* 2017; **127**: 2930–2940.

26. Budczies J, Allgäuer M, Litchfield K, *et al*. Optimizing panel-based tumor mutational burden (TMB) measurement. *Ann Oncol* 2019; **30**: 1496–1506.

27. Chang H, Sasson A, Srinivasan S, *et al*. Bioinformatic methods and bridging of assay results for reliable tumor mutational burden assessment in non-small-cell lung cancer. *Mol Diagn Ther* 2019; **23**: 507–520.

28. Campbell BB, Light N, Fabrizio D, *et al*. Comprehensive analysis of hypermutation in human cancer. *Cell* 2017; **171**: 1042–1056.e10.

29. Liberzon A, Birger C, Thorvaldsdóttir H, *et al*. The Molecular Signatures Database (MSigDB) hallmark gene set collection. *Cell Syst* 2015; **1**: 417–425.

30. Marabelle A, Le DT, Ascierto PA, *et al*. Efficacy of pembrolizumab in patients with noncolorectal high microsatellite instability/mismatch repair-deficient cancer: results from the phase II KEYNOTE-158 study. *J Clin Oncol* 2020; **38**: 1–10.

31. Germano G, Lamba S, Rospo G, *et al*. Inactivation of DNA repair triggers neoantigen generation and impairs tumour growth. *Nature* 2017; **552**: 116–120.

32. Mouw KW, Goldberg MS, Konstantinopoulos PA, *et al*. DNA damage and repair biomarkers of immunotherapy response. *Cancer Discov* 2017; **7**: 675–693.

33. Ablasser A, Goldeck M, Cavlar T, *et al*. cGAS produces a 2'-5'-linked cyclic dinucleotide second messenger that activates STING. *Nature* 2013; **498**: 380–384.

34. Corrales L, McWhirter SM, Dubensky TW Jr, *et al*. The host STING pathway at the interface of cancer and immunity. *J Clin Invest* 2016; **126**: 2404–2411.

35. Härtlova A, Erttmann SF, Raffi FA, *et al*. DNA damage primes the type I interferon system via the cytosolic DNA sensor STING to promote anti-microbial innate immunity. *Immunity* 2015; **42**: 332–343.

36. Ma Z, Damania B. The cGAS-STING defense pathway and its counteraction by viruses. *Cell Host Microbe* 2016; **19**: 150–158.

37. Pantelidou C, Sonzogni O, De Oliveria Taveira M, *et al*. PARP inhibitor efficacy depends on CD8(+) T-cell recruitment via intratumoral STING pathway activation in BRCA-deficient models of triple-negative breast cancer. *Cancer Discov* 2019; **9**: 722–737.

38. Sen T, Rodriguez BL, Chen L, *et al*. Targeting DNA damage response promotes antitumor immunity through STING-mediated T-cell activation in small cell lung cancer. *Cancer Discov* 2019; **9**: 646–661.

39. Zitvogel L, Galluzzi L, Kepp O, *et al*. Type I interferons in anti-cancer immunity. *Nat Rev Immunol* 2015; **15**: 405–414.

40. Sato H, Niimi A, Yasuhara T, *et al*. DNA double-strand break repair pathway regulates PD-L1 expression in cancer cells. *Nat Commun* 2017; **8**: 1751.

41. Yélamos J, Moreno-Lama L, Jimeno J, *et al*. Immunomodulatory roles of PARP-1 and PARP-2: impact on PARP-centered cancer therapies. *Cancers (Basel)* 2020; **12**: 392.

42. Fridman WH, Zitvogel L, Sautès-Fridman C, *et al*. The immune contexture in cancer prognosis and treatment. *Nat Rev Clin Oncol* 2017; **14**: 717–734.

43. Le DT, Uram JN, Wang H, *et al*. PD-1 blockade in tumors with mismatch-repair deficiency. *N Engl J Med* 2015; **372**: 2509–2520.

44. Mehnert JM, Panda A, Zhong H, *et al*. Immune activation and response to pembrolizumab in POLE-mutant endometrial cancer. *J Clin Invest* 2016; **126**: 2334–2340.

45. Peng G, Chun-Jen Lin C, Mo W, *et al*. Genome-wide transcriptome profiling of homologous recombination DNA repair. *Nat Commun* 2014; **5**: 3361.

46. Bracken AP, Ciro M, Cocito A, *et al*. E2F target genes: unraveling the biology. *Trends Biochem Sci* 2004; **29**: 409–417.

47. Cook R, Zoumpoulidou G, Luczynski MT, *et al*. Direct involvement of retinoblastoma family proteins in DNA repair by non-homologous end-joining. *Cell Rep* 2015; **10**: 2006–2018.

48. Patel AG, Sarkaria JN, Kaufmann SH. Nonhomologous end joining drives poly(ADP-ribose) polymerase (PARP) inhibitor lethality in homologous recombination-deficient cells. *Proc Natl Acad Sci U S A* 2011; **108**: 3406–3411.

49. Garsed DW, Alsop K, Fereday S, *et al*. Homologous recombination DNA repair pathway disruption and retinoblastoma protein loss are associated with exceptional survival in high-grade serous ovarian cancer. *Clin Cancer Res* 2018; **24**: 569–580.

SUPPLEMENTARY MATERIAL ONLINE

Figure S1. Analysis of HRDsum in subtypes of breast and ovarian cancer